Design of a low-cost modular actuator for humanoid robotics

William Duckitt [1*], *João* de Freitas [2*]

[1] Department of Electrical & Electronic Engineering, University of Stellenbosch, South Africa
[2] Department of Electrical & Electronic Engineering, University of Stellenbosch, South Africa

Abstract. A modular electromechanical actuator (EMA) is developed for humanoid robotic applications, targeting cost-effective and scalable joint actuation. The actuator employs multiple brushed DC motors coupled with a two-stage planetary gearbox to achieve sufficient torque for humanoid joints while maintaining low cost and manufacturability. The design prioritizes modularity to accommodate various robotic configurations, with considerations for material selection, additive manufacturing, and control implementation. Performance evaluations confirm effective load-bearing capacity and operational efficiency. Future iterations aim to integrate brushless motors and advanced cooling mechanisms to enhance robustness. This work contributes to the effort of creating accessible and high-performing actuators for humanoid robots.

1 Introduction

The advancement of humanoid robotics relies on the availability of high-performance yet cost-efficient actuators. Traditional actuation systems are often expensive, limiting their accessibility in research and development, [1]. Addressing this limitation, our study [2] explores a low-cost EMA designed to function as a control joint for humanoid robots. The actuator integrates accessible materials, additive manufacturing, and an affordable control system to optimize cost-effectiveness without compromising performance.

Humanoid robots have transformative potential across multiple industries [3], yet commercial actuators often exceed budgetary constraints for research and implementation in these industries. Furthermore, the rise of DIY robotics and open-source hardware shows a collective movement towards democratizing such technologies. By making use of accessible materials, additive manufacturing (such as 3D printing), and innovative design approaches, it is possible to create robotic actuators that meet the demands of various applications without the associated high costs.

[*1]William Duckitt: wdduckitt@sun.ac.za [*2]João de Freitas: 24085898@sun.ac.za

1.1 Contributions

Novel four-motor parallel configuration with a cost-effective approach using multiple small, brushed DC motors to achieve higher torque output with a fully 3D-printable modular design, complete actuator housing, and gearbox system.

1.2 Background

Traditional actuation methods include linear actuators, hydraulics, and pneumatic systems. These systems will offer great load manipulating forces; however, they are bulky and do not provide the necessary responsiveness or agility needed in humanoid robotics, as their ability to replicate natural human motion is limited. They would also require additional systems such as compressors or fluid systems, creating more points of maintenance and potential failure. In contrast, electromechanical actuators are becoming the industry standard in robotics as they offer precise and sophisticated control, achieving lifelike articulation of humanoid joints with sufficient load-bearing capacity all within a confined package. [1]

We aim to develop an affordable, easily manufacturable EMA suitable for a humanoid robot's elbow joint in this project, explicitly avoiding any exotic materials or complex control. The goals are to achieve useful torque and precision at minimal cost by using modular, 3D-printed components and available motors, while maintaining durability and repeatability. Within these limits, we justify design decisions by cost, availability, and performance trade-offs.

1.3 Related work

The MIT's Cheetah 3 actuator [4] inspired the modular approach of this project. Katz demonstrated that an actuator built with off-the-shelf drone motor parts and custom planetary gearbox allowed for a continuous torque of 6.9 Nm, and a peak torque of 17 Nm. Their actuator could accomplish dynamic capabilities, such as their quadruped performing 360° backflips. While effective, Katz's custom-fitted BLDC motor and machined gearbox increases costs. Their main challenge included thermal limitations since winding temperatures would reach excessive levels that limited continuous operation. Gearbox friction and cogging torque also affected precision. Table 1 shows the characteristics of their developed Cheetah 3 actuator.

Table. 1. Specifications of MIT Cheetah 3 actuator [4]

Mass	480 g
Dimensions	96 mm O.D., 40 mm axial length
Maximum Torque	17 Nm
Continuous Torque	6.9 Nm
Maximum Output Speed	40 rad/s or 6.4 rev/s @ 24 volts
Maximum Output Power	+250 / -680 watts

Bledt et al. [5] showed the value of quasi-direct drive (very low gear ratio) in high-speed legged robots. Their Cheetah 3 actuators achieved high torque density by using a large rotor and only 7.67:1 gearing. Their work highlights that a high torque per mass often outweighs gearbox complexity in dynamic tasks.

Berri et al. [6] designed a fully 3D-printed planetary gearbox for an actuator test bench. They noted the limitations of fused-filament materials (namely lower strength and precision) and suggested dual-load paths (such as disc brakes) or support bearings to improve durability. They were able to achieve a high ratio planetary gearbox in a small form-factor using FDM printing and a bearingless construction to minimize moving parts, with practical lessons regarding 3D printing constraints, such as managing overhangs and support structure.

The Berkeley Humanoid Lite project [7] investigates cost-driven humanoid design. Its authors used a modular 3D-printed gearbox in each joint, fabricated from cycloidal-gear modules (to counteract plastic weakness). Their robot's total cost was kept under $5000 by using off-the-shelf microcontrollers and motors. They also found it necessary to do extensive testing to ensure 3D-printed plastic parts survived repetitive motion.

A framework named TORP (The Open Robot Project) [8] proposes a modular approach to robotic development across electrical, mechanical, and computational dimensions by decoupling robot cores to form modular parts through a shared specification set. This is done to self-contain modules and provide independent power regulation, embedded low-level control, networked coordination, and standardized mechanical plugs, enabling hardware and software reuse across heterogeneous robot platforms. A comparative analysis of human joints versus HUBO (a humanoid robot by the Korea Advanced Institute of Science and Technology) actuators, as seen in Table 2, revealed that robotic actuators underperform in both power and speed; human muscle-specific power (roughly 500 W/kg) substantially exceeds that of contemporary actuators (roughly 150 W/kg), establishing quantitative targets for future actuator design. Human joints, such as elbows requiring 40 Nm torque, set performance benchmarks.

Table. 2. Specifications of human joints relative to robotic joints [8]

Joint	Human Power (W)	Velocity (RPM)	Torque (N·m)	HUBO Power (W)
Wrist	30	150	20	22
Elbow	110	150	40	90
Ankle	50	150	110	180
Shoulder	110	350	70	270
Knee	600	150	160	300
Hip	600	300	140	330
Estimated	3 000	-	-	2 384

This shows the need to tailor actuator specifications based on the joint requirements. Different joints, like such the shoulder versus elbow, require distinct specifications, emphasizing the need of designing modular actuators for adaptable applications.

2 System architecture

This section discusses the overall design of the system.

2.1 System design

The full system diagram for the actuator can be seen in Figure 1.

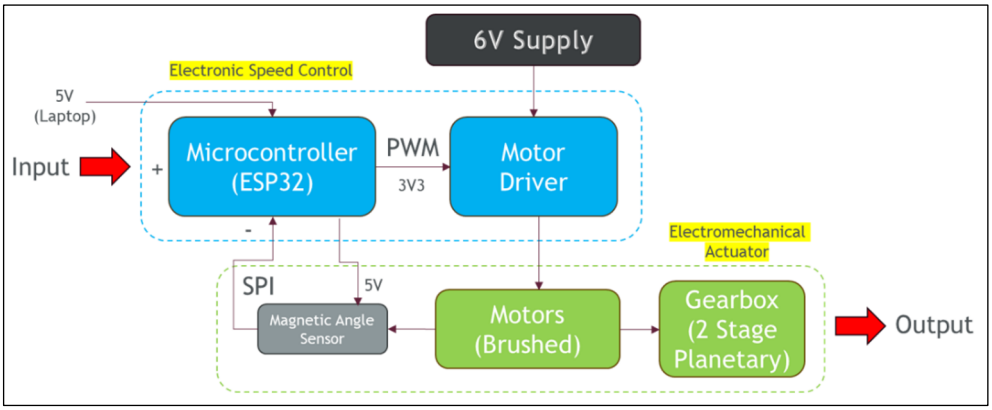

Fig. 1. System diagram of the full electromechanical actuation system

Our concept uses four small, inexpensive (~R23) DC motors, known as “TT motors”, being coupled to a central gear. Each motor already includes a small gearbox (48:1 geartrain), leading to an output torque of under 0.2 Nm per motor and a rated speed of over 200 RPM, according to its datasheet. Driving the four motors in parallel should allow us to multiply the torque in theory, and the central shaft should yield ~0.8 Nm at the output (neglecting losses), a common practice in the hobbyist community [9]. This central shaft leads to a 2:1 planetary gear reduction for the first stage, and the output is connected to a second planetary stage with a ratio of 4.5:1, giving a total gear reduction of 9:1.

The system architecture integrates four brushed DC geared motors mounted around the output shaft with a central spur gear driven by these motors, with a final gear ratio of 9:1 where the output couples to the joint flange. A dual H-bridge driver based on the L298N operates at 6V and delivers 2A per channel in continuous operation for a total of 4A, with the four motors divided into two parallel banks each driven by one H-bridge. An ESP32 microcontroller provides closed-loop control and USB connectivity while a magnetic encoder utilizes a diametric magnet which enables angular feedback for precise closed-loop operation. The four-motor configuration combined with the single H-bridge motor driver significantly enhanced affordability, reducing costs by nearly 10-fold compared to BLDC motor systems with FOC drivers. Small DC geared motors are readily available online and require only simple H-bridge controllers like the L298, eliminating the need for complex three-phase FOC controllers. Although brushed motors exhibit lower efficiency and

experience brush wear, their brush life remains acceptable for prototype applications. The custom 3D-printed housing holds the motors and gearbox with printed inserts to precisely locate shafts and bearings, which can all be assembled and disassembled chronologically with ease. All major structural parts (gearbox walls, motor mounts) were printed in PLA, chosen for stiffness and ease of printing. Extra material and fillets around screw bosses were placed to reduce stress concentrations. The actuator can be seen in its final form-factor seen in Figure 2.a, with a cross-sectional view in Figure 2.b, and an exploded view in Figure 3.

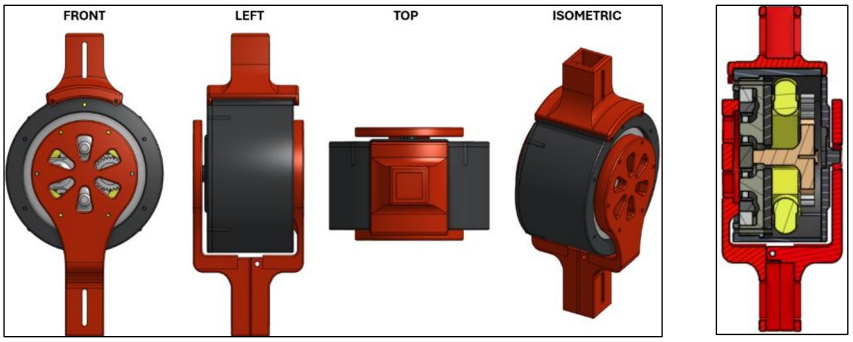

(a) **(b)**

Fig. 2. (a) Multiview projections of brushed motor actuator, and **(b)** a cross-sectional view

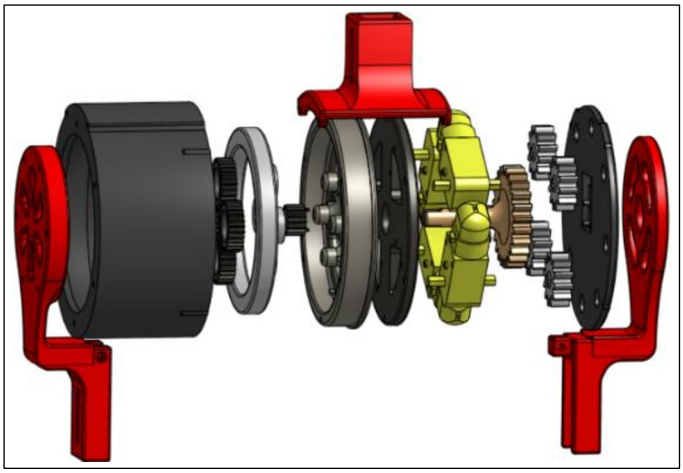

Fig. 3. Exploded view of actuator

2.2 Mechanical design

For the mechanical design of the EMA system, we employed a Star Type planetary gearbox, where the carrier is fixed. The sun gear (16 teeth) acts as the input, driving the internal ring gear (72 teeth) via four planet gears (28 teeth each). Three critical conditions ensure proper gear functionality [10]: the center distance must match the sum of the sun and twice the planet gear teeth (Equation 1), the number of teeth on the sun and ring gears must be divisible by the number of planet gears for even spacing (Equation 2), and the planet gear teeth count must prevent interference during meshing (Equation 3). The first planetary stage with the brushed motors has a -2:1 reduction ratio (reversed output direction), and the ratio for the second stage is a -4.5:1 reduction (Equation 4), which together combines into a total 9:1 reduction. In the following equations, z_a is the number of sun gear teeth, z_b is the number of each planet gear, z_c is the number of ring gear teeth, N is the amount of planet gears, and G is the transmission ratio.

Center distance matching:

$$z_c = z_c + 2z_c = 16 + 2(28) = 72 \tag{1}$$

Evenly spaced planet gears:

$$\frac{z_a + z_c}{N} = \frac{16 + 72}{4} = 22 \tag{2}$$

Interference prevention:

$$z_b + 2 \; < \; (z_a + \; z_b) \sin\left(\frac{180°}{N}\right) \tag{3}$$

$$\rightarrow \quad 28 + 2 = 30 \; < \; (16 + 28) \sin(45°) = 31.51$$

Transmission ratio:

$$G = \; -\frac{z_c}{z_a} = \; -\frac{72}{16} = \; -4.5 \tag{4}$$

The housing integrates rectangular extrusions and skirting to secure bearings, ensuring operational stability. A central shaft connects both planetary stages, with the first-stage sun gear embedding a diametric magnet aligned to a magnetic angle sensor within a 3 mm tolerance. Modularity is achieved via screw holes optimized for structural integrity with minimal fasteners. Wire routing and material efficiency are enabled by internal channels.

3D printing utilized critical settings such as a wall line count of 5 and 50–75% gyroid infill density to balance rigidity and material efficiency. The gyroid pattern ensures uniform strength under multidirectional loads. Extrude depth (10 mm) and full root fillets enhance gear durability. Tolerancing analysis revealed minimal shrinkage in larger components (e.g., 0.4% outer diameter deviation in a 100 mm bearing insert) but significant deviations in smaller parts (e.g., 13% oversizing in M3 screw holes).

2.3 Torque optimization

The modular nature of the actuator allows its integration into various humanoid robotic joints, such as the elbow or shoulder. The actuators are classified into four torque categories, each suited to different humanoid robotic joints, ranging from low-torque wrist applications to high-torque knee actuation. The modular nature of the actuator allows its integration into various humanoid robotic configurations, with scalability across different joint types. Figure 4 demonstrates this with class 1 and 3 actuators.

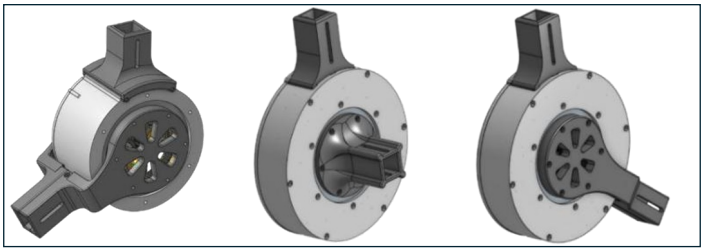

Fig. 4. Class 1 revolute joint (left), class 3 orthogonal revolute joint (middle) and revolute joint (right)

2.4 Electronic design and control system

The hardware design integrates an ESP32 microcontroller, AS5147P magnetic position sensor, IBT-2 motor driver, and four brushed DC motors. The ESP32 serves as the central controller, managing communication with the motor driver and sensor. GPIO pins 32 (RPWM) and 33 (LPWM) generate PWM signals for motor direction, while GPIO 25 enables the driver. SPI communication with the AS5147P sensor uses GPIO 18 (CLK), 19 (MISO), 23 (MOSI), and 5 (CSn) for real-time rotational feedback. These pins were selected for hardware SPI compatibility and efficient data exchange. This is seen in Figure 5.

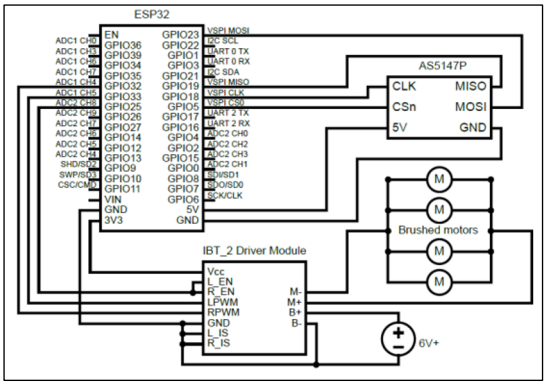

Fig. 5. Electronic speed control architecture

The AS5147P sensor tracks the first-stage sun gear's position via a diametric magnet, calibrated to account for the 4.5:1 gear reduction. The sensor alignment must be within a 3

mm tolerance of the diametric magnet. The IBT-2 motor driver employs BTS7960 chips to control motor speed and direction. Initial issues included a missing ground connection at header P1 and unifying both enable pins for proper functionality (L_EN and R_EN) as seen in Figure 4, which was resolved by manually grounding the PSU and connecting both enable pins to a single GPIO pin.

We supply power by using a GPD-3303 PSU, limited to 6 V, and up to 7.2 V for stress testing. Four brushed DC motors drive the planetary gearbox, each tested for torque and speed. Torque was measured by suspending weights at 10 cm from the gear center for both individual motor measurements and the full actuator, using the equation:

$$T_i = d \times w_i \times g \tag{5}$$

where T_i is the motor's torque, d = 0.1m, w_i is the weight, and g is gravity. Total actuator torque combines individual motor torques multiplied by the 9:1 gear ratio:

$$T_{total} = \sum_{i=1}^{4} T_i \times 9 = 6.192\ Nm \tag{6}$$

which will be our expected output torque. Output speed is derived from the minimum motor speed (203 RPM) divided by the gear ratio

$$N_{output} = \frac{203.0}{9} = 22.56\ RPM \tag{7}$$

Testing revealed motor performance variations, addressed through iterative calibration. The system prioritizes modularity, enabling component replacement and scalable integration into robotic joints.

2.5 Firmware design

The actuator's firmware, implemented on the ESP32 microcontroller, combines real-time sensor feedback, PID control, and user interfacing. A closed-loop control system processes AS5147P magnetic encoder data via SPI to generate PWM signals for motor control, maintaining position accuracy within operational limits.

The software features:

- Proportional control with dynamic motor adjustments
- Error-handling routines with speed/position thresholds
- Automatic startup calibration for zero-position alignment
- Serial interface for command input (target angles, calibration) and diagnostics
- Static friction compensation for smooth startup

The system balances real-time responsiveness with user configurability, achieving stable control within the actuator's mechanical constraints.

3 Methodology

Calibration and instrumentation. Dimensional checks used a 0.01 mm-resolution digital calliper. Speed was measured with a tachometer (±0.05% accuracy). Masses were measured on a digital scale (0.01 g resolution). A handheld multi-meter monitored voltage and current.

Experimental procedures made use of a 3D printed training arm with a notch at 0.10 m from the pivot standardized load application, as seen in Figure 6.a. Each of the four motors was first characterized independently: a rod fixed to the output gear carried a bottle ballast; water mass was incremented in ~2-3 g steps at a 0.10 m lever arm to vary torque, while current and speed were recorded. Torque per motor was computed by:

$$T_i = d \cdot w_i \cdot g \tag{7}$$

Each motor was measured and slightly varies, as seen in Table 3. Stall current, holding torque, effective torque, and speed (no load) were measured. Each test was repeated 5 times to confirm repeatability, and then the averages were tabulated.

Table 3. Specifications of each TT motor

Motor	Holding Torque (Nm)	Effective Torque (Nm)	Stall Current (A)	Average Speed (RPM)
1	0.0694	0.164	1.08	218.7
2	0.0568	0.182	1.09	211.3
3	0.0592	0.183	1.13	210.0
4	0.0484	0.159	1.11	203.0

The assembled EMA was evaluated the same. Output speed was measured at the arm and compared to the motor-side speed to infer gearbox efficiency, acknowledging losses from friction and alignment. Assembly/disassembly times were recorded during timed maintenance cycles; print time and filament usage were estimated from the slicer to quantify manufacturing effort. Structural margin was probed via arm failure torque tests on 3D-printed geometries matching the actuator arm. This methodology yielded a consistent, instrumented pathway from unit-motor characterization to system-level validation aligned with the conference paper's architecture and metrics.

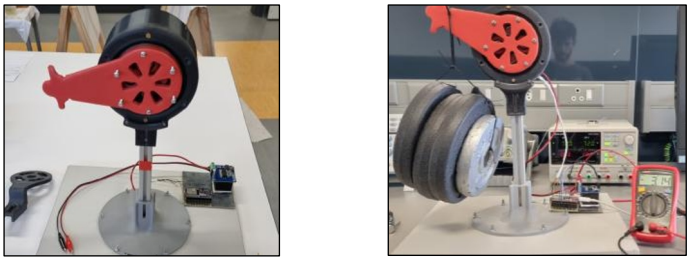

(a) **(b)**

Fig. 6. (a) Photo of built actuator with training arm, and **(b)** actuator picking up 6 kg at 10 cm

4 Results

Table 4 summarizes the comprehensive performance metrics obtained through testing.

Table 4. Performance and assembly metrics for the actuator

Parameter	Value	Description
Effective Torque	4.41 Nm	Consistent torque output during operation
Max Torque	5.89 Nm	Maximum observed torque
Output Speed	16.09 RPM	Actuator arm rotational speed
Stall Current	3.14 A	Total stall current of four motors in parallel
Max Output Power	22.61 W	Peak power output, calculated as $P = V \times I$
Efficiency	71.32%	Output speed over minimum motor speed
Assembly Time	12 min	Time required to assemble the actuator
Disassembly Time	8 min	Time required to disassemble the actuator
Dimensions	124 mm OD, 78 mm W	Actuator dimensions (excluding holds)
Total Print Time	79.1 hours	Cumulative 3D printing time for all parts
Total Filament Length	190.3 m	Total filament length used in 3D printing
Failure Torque of Arm	15.7 Nm	Torque required to break one lever
Cost	R1035.91	Cost of all components present in the system

We observed a maximum torque output of nearly 6 Nm under stall conditions, with consistent effective torque of 4.41 Nm during prolonged operation. Holding torque measured 2.03 Nm without power. The output arm rotated at 16.09 RPM under no load, achieving 71.32% system efficiency from the expected 22.56 RPM from Equation 7. These metrics confirm reliable torque for low-speed humanoid joint applications. An analysis of individual motor performance (Table 3) and system-level results (Table 4) validates the actuator design approach. The combined effective torque from all four motors totals 0.688 Nm, which when amplified by the 9:1 gear reduction theoretically yields 6.192 Nm. The measured effective torque of 4.41 Nm represents 71.2% of this maximum, with losses attributed to gearbox friction, bearing resistance, and minor gear misalignments.

Load-bearing tests validated structural reliability, sustaining a 4.5 kg load at 10 cm for intermittent operation over a week. Failure testing revealed a breaking torque of 15.7 Nm, equivalent to a 20 kg load at 8 cm. Extended operation caused slight degradation in speed and torque due to motor wear. Position control accuracy remained within 1° error during positional sweeps, accounting for gear backlash.

Durability testing showed no significant wear or backlash increase on mechanical parts. Manufacturing metrics include 79.1 hours of print time, 190.3 meters of PLA filament, and assembly/disassembly times of 12 and 8 minutes, respectively. Modular design enabled straightforward assembly using common tools. Total component costs amounted to R1,035.91, with ball bearings (R477.70) and electronics (R558.21) as major contributors.

5 Conclusion

A modular, low-cost EMA was designed and validated for a humanoid robot, achieving effective torque and efficiency while maintaining affordability. The actuator serves as a foundational step toward developing scalable and accessible robotic actuation systems, enabling broader adoption of humanoid robotics research. Key limitations include the thermal limits of PLA (deformation >80 °C) and a minor gearbox backlash which caused minor positioning inaccuracies. The brushed motors also exhibited performance decay under prolonged testing conditions. Nearly half of the actuator cost can be attributed to ball bearings, showing that there is potential to dramatically decrease costs by finding cheaper suppliers or with a bearingless approach. Key findings include the viability of a majority 3D-printed gearbox for repetitive loads and prioritizing localized stress points to be machined (such as the sun gear of a planetary gearbox, experiencing most of the translated force). In summary, the project confirms that affordable, modular joint actuators can be achieved with off-the-shelf and 3D-printed components, opening the door to more accessible humanoid robotics.

5.1 Future work

Future work should explore metal 3D printing or machining, advanced cooling, and higher-efficiency motors while retaining modularity. Future work could involve the transition to metal components, exploring cooling methods, and the use of three-phase motor designs with FOC control to enhance overall performance for broader applications. Additionally, implementing EtherCAT could offer advanced communication capabilities for synchronized control across multiple actuators. Investigating alternative gearbox designs with higher gear reductions may yield better torque amplification, while more layered or optimized space configurations could lead to improved compactness and modularity.

5.2 Recommendations

Transitioning to metal components is advisable to improve durability, which will address limitations in component wear during extended testing. Exploring alternative gearbox configurations with higher gear reductions is recommended to amplify torque output further, particularly in applications demanding greater load-bearing capabilities, and with the incorporation of a three-phase motor design could enhance efficiency and output for dynamic movements. Otherwise, selecting higher torque and speed rated brushed motors could enhance the actuator’s performance, potentially allowing it to surpass commercially available actuators in terms of torque and speed relative to cost.

References

1. Yuan,Z. *Current status and prospects of actuator in robotics*, Applied and Computational Engineering, **11**, 181-191 (2023)
2. J.P. De Freitas, *Designing and Implementing a Low-Cost Modular Actuator as a Control Joint for a Humanoid Robot*, Stellenbosch University (2024)
3. V. Cook, M. H. Lee, Y. Liu, Humanoid robots 101, Bank of America Institute, 29 April 2025. [Online]. Available: https://institute.bankofamerica.com/economic-insights/consumer-morsel-housework.html
4. B.G. Katz, *A Low Cost Modular Actuator for Dynamic Robots*, Master's thesis, Massachusetts Institute of Technology, Cambridge, (2018), [Online]. Available: https://dspace.mit.edu/handle/1721.1/118671
5. G. Bledt, M. J. Powell, B. Katz, J. D. Carlo, P. M. Wensing, and S. Kim, MIT Cheetah 3: Design and Control of a Robust, Dynamic Quadruped Robot, in Proceedings of the IEEE/RSJ International Conference on Intelligent Robots and Systems (IROS), Madrid, Spain, 1–5 October 2018, pp. 2245–2252 (2018).
6. P.C. Berri, M.D. Dalla Vedova, P. Maggiore, G. Riva, "Design and development of a planetary gearbox for electromechanical actuator test bench through additive manufacturing", Actuators, vol. **9**, no. 2, p. 35 (2020)
7. Y. Chi, Q. Liao, J. Long, X. Huang, S. Shao, B. Nikolic, Z. Li, and K. Sreenath, Demonstrating Berkeley Humanoid Lite: An Open-source, Accessible, and Customizable 3D-printed Humanoid Robot, arXiv preprint arXiv:2504.17249v1 (2025). [Online]. Available: https://arxiv.org/abs/2504.17249v1
8. A. da S. Simões, E. L. Colombini, J. P. Matsuura, and M. N. Franchin, J. Intell. Robot. Syst. **66**, 3–22 (2012).
9. RLT, *Using two BRUSHED motors on one controller*, Endless Sphere Forums (2008), [Online]. Available: https://endless-sphere.com/sphere/threads/using-two-brushed-motors-on-one-controller.3181/
10. Kohara Gear Industry, *Gear systems – planetary gear system*, [Online]. Available: https://khkgears.net/new/gear_knowledge/gear_technical_reference/gear_systems.html